VISUALIZATION OF THE TOPOLOGY OF THE LARGE-SCALE STRUCTURE IN THE PLANAR TURBULENT JET.

S.V. Gordeyev[1] **, F.O. Thomas**[2]

Keywords: *turbulent jet, coherent structure, wavelets, proper orthogonal decomposition*

ABSTRACT

Visualization of the large-scale coherent structure in fully turbulent flows is notoriously difficult owing to the presence of fine-scale fluctuations and inability to inject markers at the appropriate phase speed. In this study, the proper orthogonal decomposition and wavelet analysis are used in combination to reveal instantaneous streamlines associated with the large-scale structure in the turbulent planar jet.

1 INTRODUCTION

Visualization of the large-scale vortical structures in any fully turbulent flow is a challenging problem. The presence of small-scale incoherent fluctuations characteristic of turbulent flows makes it difficult to visually extract any information regarding the flow topology of the underlying large-scale organized motions. In addition, these structures convect downstream and the introduction of a flow marker like smoke or dye at *stationary point(s)* does not necessarily reveal any flow pattern because of a mismatch in phase speeds. Thus, the development of sophisticated experimental data extraction combined with proper data acquisition is necessary, if the dynamics and topology of the large-scale structures in the turbulent flow are to be visualized.

In this paper, the fully turbulent planar jet is chosen as a candidate flow for visualization of the topology of the underlying large-scale structures. One of the first indications of large-scale structure in the planar turbulent jet was reported by Goldschmidt and Bradshaw [1] and later by Everitt and Robins [2] and Cervantes and Goldschmidt [3] who observed negative time-averaged correlation between streamwise velocity fluctuations on opposite sides of the jet centerline. Oler and Goldschmidt [4] suggested that such correlation measurements are consistent with the presence of large-scale coherent structures in the similarity region of the planar jet. Detailed iso-correlation contour maps based on both streamwise and lateral velocity fluctuations as obtained in different jet facilities by Mumford [5], Antonia et al [6] and Thomas and Brehob [7] exhibit a remarkable likeness and appear consistent with the existence of a large-scale structural array in the planar jet similarity region. The study by Antonia et al [6] was performed in a heated jet and the existence of laterally coherent temperature fronts was used as the basis for a conditional sampling

Author(s): [1]*Department of Aerospace and Mechanical Engineering, University of Notre Dame, IN, 46556, USA*
[2]*Department of Aerospace and Mechanical Engineering, University of Notre Dame, IN, 46556, USA*

Corresponding author: Flint O. Thomas, Department of Aerospace and Mechanical Engineering, University of Notre Dame, IN, 46556, USA, E-mail: Flint.O.Thomas.1@nd.edu

scheme. The resulting coherent structure topology inferred from this method was suggestive of an antisymmetric structural array.

Thus, while time-average correlation measurements suggest the presence of the large-scale structure in the planar jet, introduction of a passive tracer of smoke to the self-similar region of the planar jet provides no indication whatsoever of large-scale organized motions. As was pointed out before, the reason for this is the presence of small-scale fluctuations which quickly diffuse any markers introduced to the flow and make the direct visualization of organized motions nearly impossible.

Several experimental techniques have been developed for the extraction of the coherent structure from turbulent shear flows and these are reviewed by Bonnet and Delville [8]. Such techniques may be broadly classified as ”conditional” or ”nonconditional”. Conditional techniques involve sampling the flow only during those intervals of time that satisfy some predetermined criterion that is deemed dynamically significant and is related to the presence of the coherent structure that is sought. One downside of these techniques is a lack of objectivity in the sense that one must have some predetermined idea regarding the structural topology in order to set the sampling criterion. In contrast, the Proper Orthogonal Decomposition (POD) proposed by Lumley [9] for investigation of the structure of inhomogeneous turbulent shear flows is an example of a nonconditional technique which is based on the two-point correlation tensor. The mathematical background behind the POD is the Karhunen-Loeve expansion as described in Karhunen [10] and Loève [11]. The analysis of turbulent flow via the POD is the subject of a recent comprehensive review by Berkooz, Holmes, and Lumley [12] and the text by Holmes, Lumley and Berkooz [13].

In an experimental context, the POD objectively extracts a complete set of spatial eigenfunctions (i.e. ”modes”) from the measured second-order cross correlation (or cross-spectral) matrix. The extracted modes serve as a set of optimal basis functions for expansion of the flow. The resulting expansion is optimal in the sense that convergence is more rapid than for any other possible basis. That is, the projection of the POD modes on the velocity field is maximized. It is generally recognized that the empirical eigenfunctions extracted by POD are intimately related to the coherent structure although the exact relationship is debated. For example, it was noted by Lumley [14] that the first POD mode represents the coherent structure only if it contains a dominant percentage of the fluctuation energy. For the purpose in this paper, the authors consider a summation of the most energetic POD modes as synonymous with the term coherent structure.

In order to obtain dynamical information regarding the coherent structure the empirically determined basis functions can be projected onto instantaneous realizations of the flow field. This allows the extraction of temporal phase coefficients for each of the modes that embodies their temporal behavior. In order to preserve phase information (and thereby realize the full potential of this technique), rakes or meshes containing multiple probes (so-called ”multipoint measurements”) are required. A comprehensive review of multipoint measurement techniques for turbulent flows and associated sampling requirements is presented by Glauser and George [15].

In this paper, the large-scale structure in the turbulent planar jet similarity region is examined by application of POD and a continuous wavelet transform. The POD spatial eigenfunctions for each of the three velocity components are extracted by means of twin cross-stream rakes of x-wire probes positioned with different spanwise separations. The reconstruction and subsequent visualization of the large-scale structure in the physical space are performed by projection of the obtained POD modes onto the instantaneous flow field realizations, obtained from three-rake experiments.

2 EXPERIMENTAL SET-UP

The experiments were conducted in the planar jet flow field facility located at the Hessert Center for Aerospace Research at the University of Notre Dame. The experimental setup was described in detail in Gordeyev and Thomas [16]. Here the authors highlight only essential aspects.

The flow is driven by a centrifugal blower that supplies air to a cubic plenum chamber with dimensions of 1.2 m per side. Inside the plenum air is forced to diffuse through a large layer of porous fiberglass insulation material which serves both to filter the air and decouple the flow from any blower pulsation. Air leaving the plenum enters a rectangular flow conditioning duct that leads to the nozzle assembly. The jet is formed by a two-dimensional nozzle contraction that takes the form of a cubic polynomial contour with zero derivative end conditions. The nozzle has a contraction ratio of 16:1 and ends in a two-dimensional slot that is $D = 1.27$ cm in width and $H = 45.7$ cm in height giving an aspect ratio (height/width) of 36:1. The longer dimension nozzle walls are contoured while the walls in the shorter dimension are flat. The flow field is formed between two horizontal confining plates of dimension 2.5 m in the flow direction and 1.61 m in width which serve to keep the base flow two-dimensional in nature. Twin sheet metal face plates mounted flush with the nozzle exit plane extend laterally to the edge of the flow field. All other sides of the flow field remain open. A series of large screens surround the jet facility in order to insure that any laboratory room air circulation has minimal effect on flow field. Since the jet was operated in a large laboratory space (353 m^2 floor area) with room ventilation fans off during experimental runs, any such effects on the flow were exceedingly small.

In this paper, x will denote the streamwise spatial coordinate which is made non-dimensional by the nozzle slot width, D. The cross-stream spatial coordinate is, y, and is made non-dimensional by the local mean velocity half-width, $b(x)$. The half-width is defined as the distance from the jet centerline to the lateral location where the local mean velocity has fallen to one-half its centerline value. The spanwise spatial coordinate extending in the direction of mean flow homogeneity is denoted z. The origin of the z-axis is chosen in the centerplane midway between the two flow field confining plates. The fluctuating velocity components corresponding to coordinates x, y, z are denoted u, v, w, respectively.

For the experiments reported, the nozzle exit velocity is $U_0 = 35$ m/sec which corresponds to a Reynolds number based on nozzle slot width of $Re_D = 28,000$. The second-order turbulence moments exhibit similarity for $x/D > 50$. The POD measurements were performed over the streamwise interval $50 \leq x/D \leq 90$. The flow is considered stationary in time and the spanwise coordinate is treated as statistically homogeneous. The cross flow direction is taken as the single inhomogeneous coordinate.

3 EXTRACTION PROCEDURE

In this section the method by which the POD spatial eigenmodes and associated eigenvalues were extracted is briefly described and some key results presented. Since this aspect of the study was the focus of Gordeyev and Thomas [16], only those aspects considered essential in providing the relevant framework for the current work are described here. The reader is referred to the cited reference for a more detailed presentation.

3.1 POD Technique

Cross-spectral measurements involving all three fluctuating velocity components at selected x/D planes in the similarity region of the jet $(50 \leq x/D \leq 90)$ were performed by means of *two* spanwise-separated rakes of eight x-wire probes each. Both of the rakes were located at the same x/D location and were oriented in the cross-stream direction, parallel to each other. The two rakes were separated in the spanwise direction by a user selected distance $z - z' = \Delta z$. Us-

ing the two rake system the cross-spectral matrix $S_{\alpha\beta}(y,y',f,\Delta z)$ was computed directly from the Fourier transformation of the individual velocity-time histories (see Bendat & Piersol [17]),

$$S_{\alpha\beta}(y,y',f,\Delta z) = \lim_{T\to\infty} \frac{1}{T} \left\langle \hat{u}^*_\alpha(y,z,f)\hat{u}_\beta(y',z',f) \right\rangle \tag{1}$$

where $\langle\cdot\rangle$ denotes an ensemble average and Greek subscripts denote a fluctuating velocity component u, v or w. The velocity measurement $u_\alpha(y,z,t)$ corresponds to the first rake and $u_\beta(y',z',t')$ corresponds to the second. Note that the x-wire probes are capable of the simultaneous measurement of either $(\alpha = u, \beta = v)$ or $(\alpha = u, \beta = w)$ depending on their orientation in the flow field. The quantity $\hat{u}_\alpha(y,z,f) \equiv \int_0^T u_\alpha(y,z,t)e^{-2\pi i f t}dt$ denotes the temporal Fourier transformation of the velocity vector for each block, T is the total time duration of the data block and the asterisk denotes a complex conjugate. A *spatial* Fourier transformation in the homogeneous z-direction provides a spanwise wavenumber-dependent cross spectral matrix,

$$\Phi_{\alpha\beta}(y,y';f,k_z) = \int S_{\alpha\beta}(y,y',f,\Delta z)e^{-ik_z\Delta z}d(\Delta z), \tag{2}$$

where k_z is a spanwise wavenumber. The matrix $\Phi_{\alpha\beta}(y,y';f,k_z)$ essentially unfolds $S_{\alpha\beta}(y,y',f,\Delta z)$ in spanwise wavenumber space.

As shown in Lumley [18], the spectral correlation tensor $\Phi_{\alpha\beta}(y,y';f,k_z)$ will be a kernel in the integral equation to find the POD modes for different frequencies f, and spanwise wavenumbers, k_z,

$$\int \Phi_{\alpha\beta}(y,y';f,k_z)\varphi^{(n)}_\beta(y';f,k_z)dy' = \lambda^{(n)}(f,k_z)\varphi^{(n)}_\alpha(y;f,k_z). \tag{3}$$

Here superscript n denotes mode number. The solution of (3) gives a complete set of orthonormal eigenfunctions $\varphi^{(n)}_\alpha(y;f,k_z)$ with corresponding positive eigenvalues $\lambda^{(n)}(f,k_z)$.

Lumley [18] has shown that for homogeneous directions POD modes are Fourier modes . Thus, if a direction x in the flow is taken as homogeneous, the eigenmodes in the x-direction are Fourier modes. Delville [19] pointed out that the POD technique can be treated as a generalization of Fourier transform in the inhomogeneous direction. Thus, POD can be viewed as a generalized low-pass filtering technique and some properties of Fourier analysis, like aliasing and filter cut-off issues can be extended for POD. For further discussion, the reader is referred to [16]

The resulting planar jet streamwise, lateral and spanwise component (i.e. u, v, and w, respectively) eigenmodes were experimentally obtained in a mixed physical - Fourier space (y,St,k_z) where y denotes the cross stream spatial coordinate, St is a Strouhal number based on the local mean velocity half-with $b(x)$ and the local jet centerline mean velocity U_m and k_z is the spanwise wavenumber. The detailed analysis and discussion of the eigenmodes and eigenvalues in the planar jet is the topic of the recent paper by Gordeyev and Thomas [16].

3.2 Wavelet Reconstruction

Any velocity realization can be represented as a sum of these experimentally determined eigenfunctions,

$$u_\alpha(y,z,t) = \sum_{n=1}^{\infty} u^{(n)}_\alpha = \sum_{n=1}^{\infty} \int\int c^{(n)}(f,k_z)\varphi^{(n)}_\alpha(y;f,k_z)\exp(2\pi i f t)\exp(ik_z z)\, df\, dk_z. \tag{4}$$

All the phase information necessary for reconstruction of the coherent structure in the physical domain resides in the coefficients $c^{(n)}(f,k)$. In order to find them, a projection of the POD modes back onto instantaneous realizations of the flow is needed. Instantaneous realizations of the flow onto which the POD eigenfunctions are to be projected were acquired with a triple x-wire rake

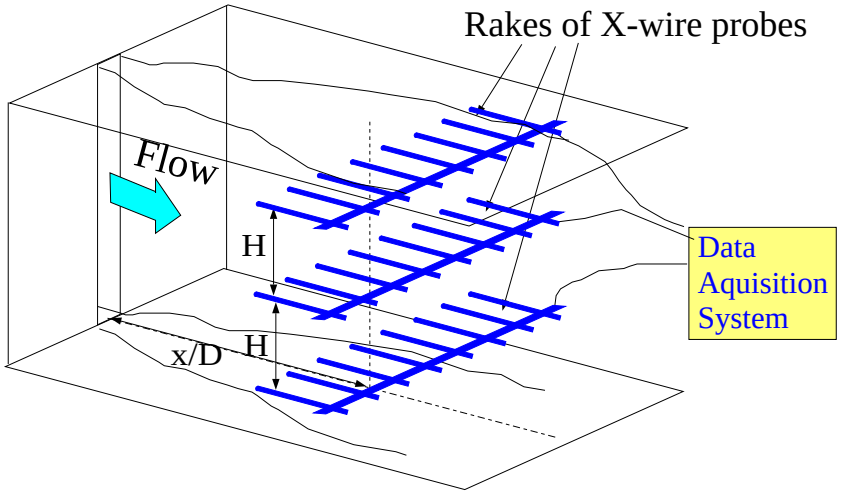

Fig. 1 Schematic of the triple x-wire rake set-up.

arrangement, Figure 1, as described in details in [24]. This allows the unambiguous extraction of the planar component of the jet structure as well as the most energetic nonplanar part. All the rakes are located at the same x/D location and extend in the cross-stream direction, parallel to each other. The rakes are separated in the spanwise direction by a distance, $H = b$. Each of the three rakes contains eight x-wire probes.

The large-scale structure is reconstructed in physical space by projection of measured u, v, and w-component POD eigenmodes onto instantaneous flow field realizations. The projection is performed by means of a continuous wavelet transform-based technique. To the authors' knowledge, the approach of using wavelet transform methods as the basis for the projection of the POD modes onto the flow (instead of Fourier methods) is unique to the study of Gordeyev and Thomas [24]. A presentation of basic wavelet theory may be found in several recent texts on the subject (e.g. Daubechies [20], Kaiser [21] and Farge [22]). The application of wavelet analysis techniques to experimental fluid mechanics is the topic of the paper by Lewalle [23].

The wavelet transformation of a continuous signal $f(t) \in L^2(\mathbf{R})$ is defined in the following way:

$$WT(\tau, a)\{f(t)\} = \widetilde{f}(\tau, a) = \frac{1}{\sqrt{a}} \int_{-\infty}^{+\infty} f(t) g^* \left(\frac{t-\tau}{a} \right) dt \tag{5}$$

where the parameter a is called a *dilatation* or *scale parameter,* τ is called a *shift parameter,* and the asterisk denotes a complex conjugate. The complex valued function $g(x)$ is called a *wavelet mother function* and it satisfies the following conditions:

$$\int g(x) g^*(x) dx < \infty \tag{6}$$

$$C(g) = 2\pi \int_{-\infty}^{+\infty} \frac{|\widehat{g}(\omega)|^2}{\omega} d\omega < \infty. \tag{7}$$

As before, the hat sign, $\widehat{(\cdot)}$ over a function denotes a Fourier transformation,

$$\widehat{g}(\omega) \equiv \int_{-\infty}^{+\infty} g(x) e^{-i\omega x} dx. \tag{8}$$

The condition (7) guarantees the existence of *the inverse wavelet transformation,*

$$f(t) = WT^{-1}(t)\left\{ \widetilde{f}(\tau, a) \right\} = \frac{1}{C(g)} \int_0^{+\infty} \int_{-\infty}^{+\infty} \frac{\widetilde{f}(\tau, a)}{\sqrt{a}} g\left(\frac{t-\tau}{a} \right) \frac{da\, d\tau}{a^2} \tag{9}$$

This investigation uses a complex Morlet wavelet mother function,

$$g(x) = e^{irx}e^{-x^2/2} - e^{-r^2/2}e^{-x^2/2}, \tag{10}$$

as the basis for the wavelet transform, with the value of $r = 1$.

3.3 Wavelet-based Reconstruction

In order to reconstruct the shape of the POD modes $\varphi_\alpha^{(n)}(y; f, k_z)$ in physical space, an inverse transform in frequency and wavenumber domains should be performed. But the POD modes are known only up to an arbitrary phase. The phase information required for reconstruction of the flow structure can be restored by projection of the POD modes onto instantaneous flow field realizations $u_\alpha(y,z,t)$ obtained at selected streamwise locations, x/D, in the similarity region of the jet. The approach outlined in the following section uses the continuous wavelet transformation to perform the projection. The reconstruction procedure consists of the following six steps:

1. A spatial Fourier transform in the z-direction is performed in order to compute $\hat{u}_\alpha(y,k_z,t) = FT\{u_\alpha(y,z,t)\}$.

2. The wavelet transformation in time (5) is calculated, $\widetilde{u}_\alpha(y,k_z;a(f),\tau) = WT(a,\tau)\{\hat{u}_\alpha(y,k_z,t)\}$.

3. Using the orthogonality of the POD modes, the coefficients (in wavelet space) $c^{(n)}(k_z;a(f),\tau)$ can be computed by projecting the POD modes onto an instantaneous realization,

$$c^{(n)}(k_z;a(f),\tau) = \int \widetilde{u}_\alpha(y,k_z;a(f),\tau)\varphi_\alpha^{(n)*}(y; f, k_z)dy.$$

4. The wavelet transform of each POD mode can be restored,

$$\widetilde{u}_\alpha^{(n)}(y,k_z;a(f),\tau) = c^{(n)}(k_z;a(f),\tau)\varphi_\alpha^{(n)}(y; f, k_z).$$

5. The inverse wavelet transform (9) provides the POD mode in a mixed Fourier-physical space,

$$\hat{u}_\alpha^{(n)}(y,k_z,t) = WT^{-1}(a,\tau)\left\{\widetilde{u}_\alpha^{(n)}(y,k_z;a(f),\tau)\right\}.$$

6. Finally, the inverse Fourier transform restores the POD modes in the physical domain,

$$u_\alpha^{(n)}(y,z,t) = FT^{-1}\{\hat{u}_\alpha^{(n)}(y,k_z,t)\}$$

The fluctuating flow field is then the sum of all POD modes,

$$u_\alpha(y,z,t) = \sum_{n=1}^{\infty} u_\alpha^{(n)}(y,z,t). \tag{11}$$

It is common to use a triple decomposition of the velocity field in order to account for the presence of the large-scale flow structure, $\mathbf{u} = \overline{\mathbf{U}} + \mathbf{u}_{LS} + \mathbf{u}_{fs}$, where $\overline{\mathbf{U}}$ is the mean velocity field, $\mathbf{u}_{LS}$ represents the large-scale coherent structure and $\mathbf{u}_{fs}$ is fine scale, phase incoherent turbulence. The authors will represent the coherent structure in terms of *a summation of the dominant POD modes*, $\mathbf{u}^{(n)}$. In addition, since the authors are interested only in the large scale motions, they neglect $\mathbf{u}_{fs}$ which are those motions that do not contribute to the cross-spectral tensor for the Δy

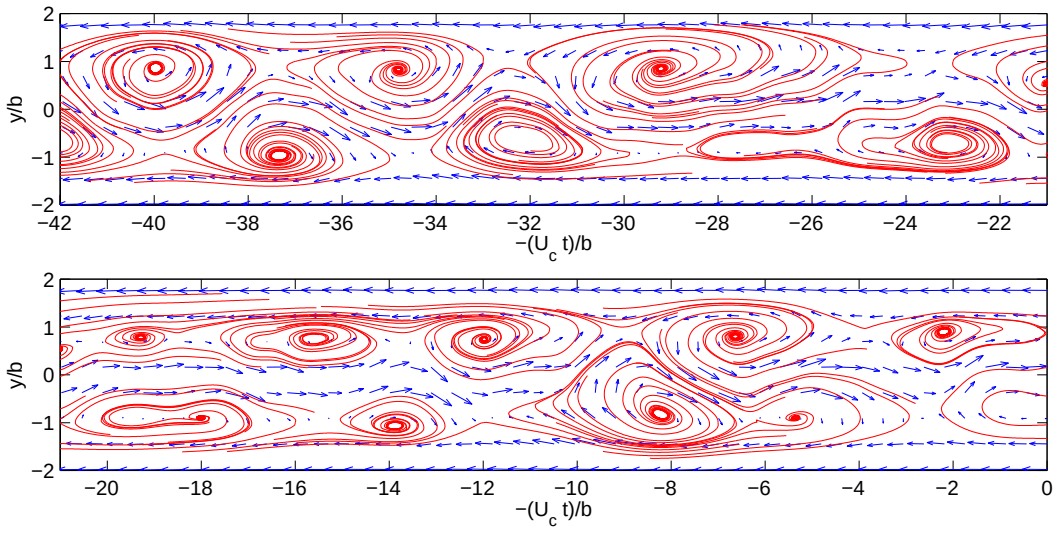

Fig. 2 Reconstructed flow field for planar coherent structure (in the moving frame of reference).

and Δz probe separations used in the experiment. The large-scale flow structure is then represented as a series consisting of the mean flow $\overline{\mathbf{U}}(y)$ and first N POD modes,

$$\widetilde{\mathbf{u}} = \overline{\mathbf{U}}(y) + \sum_{n=1}^{N} \mathbf{u}^{(n)}. \tag{12}$$

Note that the mean flow is time-independent and thus is orthogonal to the POD modes. From (12) it follows that the mean flow can be treated as *the dominant POD mode*. The remaining POD modes can be viewed as *perturbations of the mean flow*. The three-rake experiment allows one to extract the planar part of the structure, as well as a dominant nonplanar part of the structure. For an extended discussion of the three-rake experiment, see [24]. The authors take $N = 3$ to reconstruct the planar structure and $N = 2$ for the non-planar structure.

4 RESULTS OF THE FLOW RECONSTRUCTION

The jet coherent structure travels with a convective speed in the range of $U_c \approx 0.60..0.65U_M$ which is approximately independent of y for the inner region of the flow $y/b < 1$. In a frame of reference moving downstream at speed U_c new variables are then defined as $x \to x - U_c t$, $y \to y$, $\mathbf{u} \to \mathbf{u} - U_c$. One way to represent the structural topology of the planar mode is to plot the velocity vector field and instantaneous streamlines of $\mathbf{u} - U_c$ as a function of lateral position y and a pseudo-spatial streamwise coordinate $x = -U_c t$.

4.1 Planar Part of the Structure

For better visualization for the flow field corresponding to the planar part of large-scale structure, the streamlines were used in addition to velocity vector plots. The extracted planar flow field was first spline interpolated throughout the region in interest. Then, streamlines were computed as a numerical solution of the streamline equation for a series of initial points located at $y/b = \pm 1$ and uniformly distributed in the streamwise direction. Each streamline equation was numerically integrated forward and backward in time using a Runge-Kutta method. This is similar to putting dots of dye in the real flow, but here we use the filtered velocity field corresponding to the first three dominant planar POD modes. Figure 2 presents a sample of both the velocity vector field and "instantaneous streamlines" associated with the planar component of the jet coherent structure

obtained by superimposing the mean flow and the first three planar POD modes. It must be remembered that this flow pattern is presented in a frame of reference moving with constant speed U_c. Both the crosstream and pseudo-spatial streamwise coordinates y and x have been non-dimensionalized by the local mean velocity half-width b. Note that the streamlines shown are actually particle path lines. However, since time is treated as equivalent to a spatial coordinate by the assumption of a frozen field convected at U_c, they may be interpreted as instantaneous streamlines.

The pattern shown in Figure 2 is characterized by a streamwise series of centers and separatrices on both sides of the jet. This clearly shows the presence of large-scale counter-rotating vortical structures on either side of the jet which are arranged approximately antisymmetrically with respect to the jet centerline. In fact, the structural arrangement shown in Figure 2 closely resembles the classic Karman vortex street arrangement, with the locations of the two vortex lines centered at approximately $y/b \approx \pm 0.85$. There is a strong interaction between structures on opposite sides of the jet in the form of lateral streaming motions that extend well across the flow. In viewing these structures it must be remembered that the POD essentially works as a spatial filter and so the small scale turbulent noise is effectively removed from the large-scale motions in the jet. This allows one to see clearly the underlying structural topology. The structural pattern shown in Figure 2 also resembles that proposed by Oler and Goldschmidt [4] in their simple kinematic model of the jet large scale structure. In conditional sampling of a heated planar jet Antonia et al [6] associated strong temperature fronts with the separatrix between adjacent structures in the jet. Although their conditional measurements were confined to a single side of the flow, there is a resemblance between aspects of their Figure 6 and the structural pattern shown in Figure 2 of this paper.

4.2 Three-Dimensional Reconstruction

In order to restore the shape of the non-planar structure in physical space, an inverse Fourier transform should be performed, $\mathbf{u}^{(n)}_{non-planar} = u^{(n)}_{\alpha}(y,z,t) = \int \widehat{u}^{(n)}_{\alpha}(y,k_z,t)\exp(ik_z z)dk_z$. Since the triple rake arrangement only allows one to obtain the planar and a single non-planar mode, the integration can be replaced by a simple multiplication of the spanwise Fourier component by a periodic function $\exp(ik_z z)$. Taking into account that the resolved spanwise wavenumber is $k_z b/2\pi = 0.5$, the final version of the spanwise velocity reconstruction will be as follows,

$$\mathbf{u}^{(n)}_{non-planar}(y,z,t) = \left\{ \widehat{u}^{(n)}(y,k_z,t)\cos(\pi z/b),\ \widehat{v}^{(n)}(y,k_z,t)\cos(\pi z/b),\ \widehat{w}^{(n)}(y,k_z,t)\sin(\pi z/b) \right\}^T \tag{13}$$

The resulting flow field is periodic in the spanwise direction with a period of $z/b = 2$. The reason the sine function appears in the w-component is because the flow field must satisfy the continuity equation $\partial u_\alpha/\partial x_\alpha = 0$.

Each POD mode can be approximated by a sum of the planar and non-planar parts, $\mathbf{u}^{(n)}(y,z,t) \approx \mathbf{u}^{(n)}_{planar}(y,t) + \mathbf{u}^{(n)}_{non-planar}(y,z,t)$. Although this is not an exact representation, it does serve to give an approximate picture of the three-dimensional velocity field associated with the POD mode.

By including the nonplanar mode, the velocity field corresponding to the coherent structure is now a function of the three coordinates (y,z,t). This poses a challenge in presenting the results. We first investigate the flow structure by looking at cross-cuts in the three planes $z/b = 0, 0.5, 1$. It follows from (13) that in these planes the effect of the non-planar POD component is maximum. In Figures 3(a), (b) and (c) the velocity vector field and 2-D instantaneous streamlines associated with the (u,v) components are plotted for each plane. For clarity, only every fourth point in the temporal direction is plotted for the velocity vector plots. In addition, the iso-contours of the amplitude of the w-component at $z/b = 0.5$ is presented in Figure 3(d). Comparison of the flow patterns shown in Figures 3(a), (b) and (c) reveal an overall similarity which suggests the

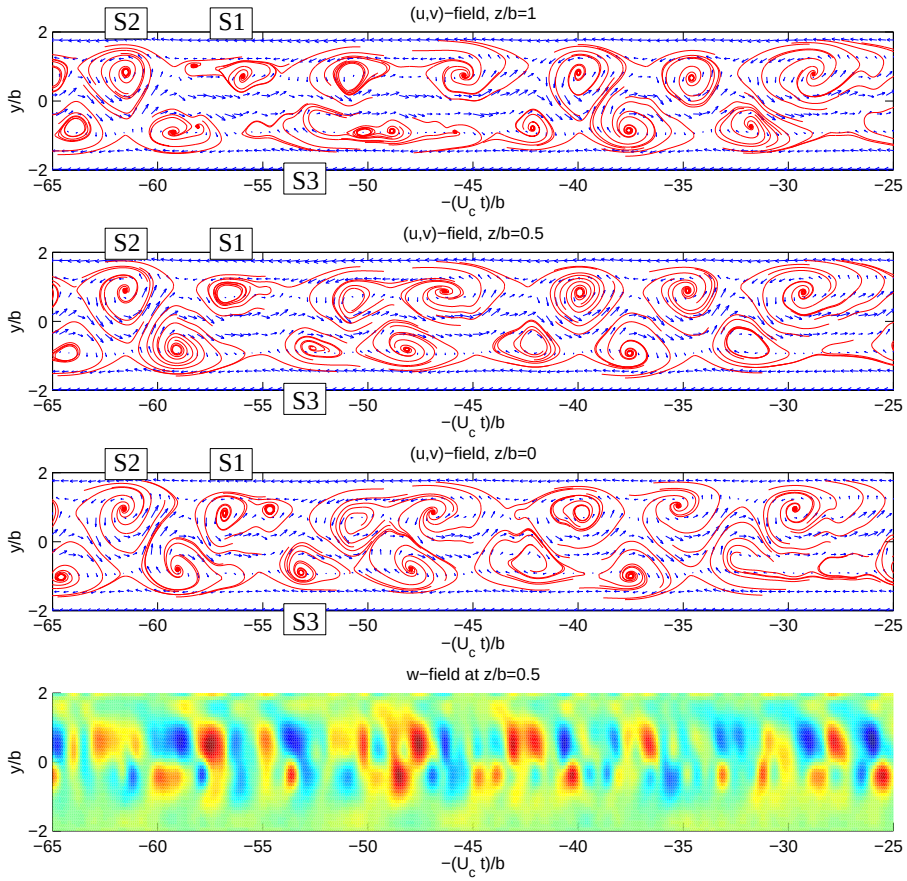

Fig. 3 The velocity field (u,v) and instantaneous streamlines of the reconstructed non-planar coherent structure $u_\alpha^{non-planar}(y,z,t)$ with first $N=2$ POD modes at **a)** $z/b=1$, **b)** $z/b=0.5$ and **c)** $z/b=0$ spanwise locations and **d)** w-component of velocity at $z/b=0.5$ (red-negative, blue-positive).

dominance of the planar mode. Closer inspection, however, reveals some important differences resulting from the nonplanar mode. First, the positions of certain vortical structures appear shifted in the different z/b planes. A particular example is labeled S1 which shows a distinct streamwise shift with changes in z. Others (e.g. S2) occur at virtually the same location. This suggests that some of the structures are tilted with respect to the z-axis while others are not. Another difference is the apparent strengthening or weakening of the z-directed vorticity associated with particular structures with changes in z. An example is labeled S3. This is also consistent with the tilting or bending of structures which will serve redistribute z-directed vorticity. Other evidence of the three-dimensional character of the flow field comes from noting that many of the centers exhibited by the planar mode streamline patterns become foci upon inclusion of the nonplanar mode. This observation is also consistent with Figure 3(d) which shows large scale, laterally coherent upward and downward (spanwise) fluid motions. Hence, Figures 3 suggest that while the planar component of the jet coherent structure is dominant, the non-planar part gives rise to its spanwise perturbation in the form of bending or tilting.

In order to investigate the structural topology, several streamlines were traced in the three-dimensional space around different vortical structures in the flow. This was done by tracking particle paths released at the same y location but in different z-planes. The particle paths are then followed in time and the resulting sheet traced. In other words, this procedure is equivalent to introducing a thin sheet from a line of smoke or dye sources extending in the spanwise direction

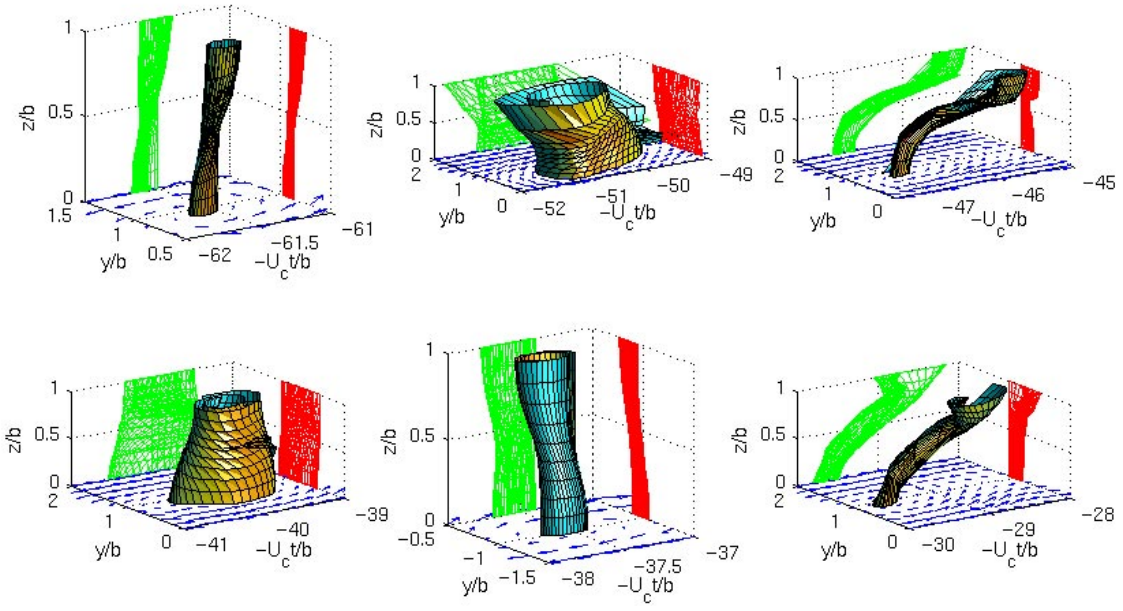

Fig. 4 Several examples of the reconstructed 3-D flow field around non-planar structures.

and observing their response to the imposed velocity field. With the assumption of a frozen field convected at U_c these particle paths become equivalent to instantaneous streamlines. To calculate these streamlines, the 3-D streamline equation was solved numerically for the velocity field (13) for 10 initial points placed uniformly along a line in the spanwise direction for a half of the period $z/b = 0..1$. A cubic spline interpolation was used in the $(U_c t, y)$ plane. The locus of obtained streamlines are plotted as a surface. A few examples are shown in Figure 4. This figure shows instantaneous streamline surfaces which wrap around a spanwise vortical structure thereby revealing the flow pattern near the core. Two projections are also shown in gray to facilitate visualizing these 3-D surfaces. Investigation of the topology of nonplanar modes shows that they indeed both tilt and bend the spanwise vortex tubes. The bending occurs primarily in the streamwise direction. The degree to which the spanwise vortices are distorted varies greatly; in some cases they are nearly streamwise oriented and in others only slight distortion of a spanwise vortex is noted. The Figure 4 reveals an obvious advantage of the low-pass filtering property of the POD technique. The most of small-scale velocity fluctuations are removed from the processed data and the topology of the large-scale structures are clearly visible. Although only a single nonplanar mode was examined, in reality a continuous spectrum of nonplanar modes $k_z b/2\pi < 1$ will distort the spanwise vortices. The result will be similar in overall topology to that presented in Figure 2 but will involve finer scale convolutions of the primary vortex tube.

REFERENCES

[1] Goldschmidt V W, and Bradshaw P. Flapping of a Plane Jet. *Physics of Fluids*, Vol. 16, pp 354-355, 1973.

[2] Everitt K W, and Robins A G. The development and structure of turbulent plane jets. *J. Fluid Mechanics*, Vol. 88, No 3, pp 563-583, 1978.

[3] Cervantes D G, and Goldschmidt V W. The apparent flapping motion of a turbulent plane jet-further experimental results. *Trans. ASME J. Fluid Eng.*, Vol. 103, pp 117-126, 1981.

[4] Oler J W, and Goldschmidt V W. A vortex-street model of the flow in the similarity region of a two-dimensional free turbulent jet. *J. Fluid Mech.*, Vol. 123, pp 523-535, 1982.

[5] Mumford J C. The structure of the large scale eddies in fully developed turbulent shear flows. Part 1, the plane jet. *J. Fluid Mech.*, Vol. 116, pp 241-268, 1982.

[6] Antonia R A, Chambes A J, Britz D, and Browne L W B. Organized structures in a turbulent plane jet: topology and contribution to momentum and heat transport. *J. Fluid Mech.*, Vol. 172, pp 211-229, 1986.

[7] Thomas F O, and Brehob E G. An investigation of large-scale structure in the similarity region of a two-dimensional turbulent jet. *Physics of Fluids*, Vol. 29, pp 1788-1795, 1986.

[8] Bonnet J P, and Delville. General concepts on structure identification. *Eddy Structure Identification*, ed. J P Bonnet. Springer-Verlag, New York, 1996.

[9] Lumley J. The structure of inhomogeneous turbulent flows. *Proceedings of the International Colloquium on the Fine Scale Structure of the Atmosphere and its Influence on Radio Wave Propagation* (ed. A.M.Yaglam, V.I.Tatarsky), Doklady Akademii Nauk SSSR, Moscow, Nauka, pp 166-178, 1967.

[10] Karhunen K. Zur Spektraltheorie Stochasticher. *Prozessa Ann. Acad. Sci. Fennicae*, Vol. 37, 1946.

[11] Loève M M. *Probability Theory*. Van Nostrand, Princeton, N.J, 1955.

[12] Berkooz G, Holmes P, and Lumley J. The proper orthogonal decomposition in the analysis of turbulent flows. *Annual Review of Fluid Mechanics*, Vol. 25, pp 539-575, 1993.

[13] Holmes P, Lumley J L, and Berkooz G. *Turbulence, Coherent Structures and Symmetry*. Cambridge University Press, 1996.

[14] Lumley J. Coherent structures in turbulence. *Transition and Turbulence*, ed. R. E. Meyer, pp 215-241, Academic Press, 1981.

[15] Glauser M N, and George W K. Application of multipoint measurements for flow characterization. *Experimental Thermal and Fluid Science*, Vol. 5, pp 617-632, 1992.

[16] Gordeyev S V, and Thomas F O. Coherent Structure in the Similarity Region of the Turbulent Planar Jet. Part 1. Proper Orthogonal Decomposition Eigenmodes and Their Self-Similarity. To appear in *J. Fluid Mech.*, 2000.

[17] Bendat J S, and Piersol A G. *Random Data*. 2nd edition, Wiley Interscience, New York, 1986.

[18] Lumley J. *Stochastic Tools in Turbulence*. Academic Press, New York, 1970.

[19] Delville J. Characterization of the organization in shear layers via the proper orthogonal decomposition. *Applied Scientific Research*, Vol. 53, No 3-4, pp 263-281, 1994.

[20] Daubechies I. *Ten Lectures on Wavelets*. Society for Industrial and Applied Mathematics, 1992.

[21] Kaiser G. *A Friendly Guide to Wavelets*. Birkhauser, 1994.

[22] Farge M. Wavelet Transforms and their Applications to Turbulence. *Ann. Rev. Fluid Mech.*, Vol. 24, pp 395-457, 1992.

[23] Lewalle J. Wavelet Analysis of Experimental Data: Some Methods and the Underlying Physics. *AIAA paper 94-2281*, 1994.

[24] Gordeyev S V, and Thomas F O. Coherent Structure in the Similarity Region of the Turbulent Planar Jet. Part 2. Structural Topology via POD Eigenmode Extraction. Submitted to *J. Fluid Mech.*, 2000.